Geochemical Perspectives Letters

Potassium isotope evidence for sediment recycling into the orogenic lithospheric mantle

Z.-Z. Wang[1,2*], F.-Z. Teng[1*], D. Prelević[3,4], S.-A. Liu[2], Z. Zhao[2]

OPEN ACCESS

doi: 10.7185/geochemlet.2123

Abstract

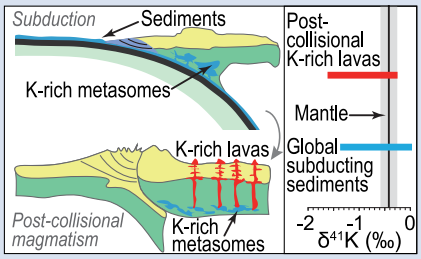

Post-collisional highly potassic magmatism in large orogenic belts has been taken as evidence for recycling of continent-derived K-rich sediments within the orogenic lithospheric mantle. Potassium isotopes may provide important insights into the origins of K in these magmas, since subducting sediments exhibit much more variable K isotopic compositions relative to the mantle. Here we report high precision K isotope data for 41 representative potassic and ultra-potassic volcanic rocks from the whole Alpine-Himalayan orogenic belt. $\delta^{41}K_{NIST\ SRM3141a}$ of these samples vary from −1.55 ‰ to −0.32 ‰, comparable to the range of global subducting sediments but significantly exceeding the range of pristine mantle defined by oceanic basalts (−0.42 ± 0.08 ‰). Monte Carlo simulation suggests this large K isotopic range can be reproduced by recycling of up to 5 % isotopically heterogeneous sediments into the depleted mantle. Our results highlight K isotopes as a potential tracer of recycled sediments in the mantle.

Received 17 February 2021 | Accepted 2 July 2021 | Published 8 September 2021

Introduction

Post-collisional potassic and ultra-potassic volcanic and plutonic rocks contain up to ~10 wt. % K_2O and are one of the most distinctive magmatic types that frequently occurred in global orogenic belts at least since the late Archean (*e.g.*, Couzinié *et al.*, 2016). Their derivation from the mantle is evident from their high MgO contents (>6 wt. %) and Mg# (>0.6), highly forsteritic ($Fo_{85–95}$) olivine phenocrysts, and the occurrence of mantle xenoliths or xenocrysts entrained by these lavas (*e.g.*, Foley *et al.*, 1987; Prelević *et al.*, 2013). Despite this, direct partial melting of mantle peridotite is unlikely to generate melts with >2 wt. % K_2O (*e.g.*, Walter, 1998). These highly potassic lavas are usually enriched in incompatible trace elements, with extreme radiogenic isotopic compositions and trace element patterns resembling those of subducting sediments (*e.g.*, Foley *et al.*, 1987; Williams *et al.*, 2004; Prelević *et al.*, 2008; Avanzinelli *et al.*, 2009; Conticelli *et al.*, 2009; Zhao *et al.*, 2009; Couzinié *et al.*, 2016). These features indicate that the recycling of continent-derived sediments into their mantle sources contributes to the peculiar K enrichment in these lavas. However, correlated relationships between K enrichment and common indices of sediment contribution in highly potassic lavas such as Th/La, Sm/La, Th/Nb, Hf/Sm and radiogenic isotopes (*e.g.*, Sr, Nd, Pb, and Os) are rarely observed (Tommasini *et al.*, 2011; Prelević *et al.*, 2013). This decoupled behaviour might reflect that (1) the budget of Th, Nb, Hf and REE in sediments is dominated by accessory minerals (*e.g.*, epidote, rutile and zircon) barely accommodating K, and (2) radiogenic isotopic compositions depend on age and time-integrated parent/daughter ratio, unrelated to K abundance in sediments.

Recent developments in high precision K isotopic analysis (≤0.06 ‰) revealed large K isotopic variation (~1.3 ‰) in sediments, which has been ascribed to low temperature processes such as chemical weathering or diagenesis (Li *et al.*, 2019; Chen *et al.*, 2020; Hu *et al.*, 2020; Huang *et al.*, 2020; Santiago Ramos *et al.*, 2020; Teng *et al.*, 2020). By contrast, high temperature magmatic processes do not significantly fractionate K isotopes (Tuller-Ross *et al.*, 2019a,b; Hu *et al.*, 2021a). Hence, potassium isotopes can potentially be used to trace sedimentary K in mantle-derived melts, which has been recently applied to explain the K isotopic variations in intracontinental basalts from northeast China (Sun *et al.*, 2020) and arc lavas from Lesser Antilles (Hu *et al.*, 2021b).

Here we report the first comprehensive K isotope dataset for representative post-collisional K-rich lavas from eight regions within the Cenozoic Alpine-Himalayan orogenic belt (AHOB; Fig. 1a). These samples are well characterised for their petrology, mineralogy, major, trace element, and radiogenic isotope geochemistry (Prelević *et al.*, 2005, 2008, 2012, 2015; Zhao *et al.*, 2009; S.-A. Liu *et al.*, 2020). They cover major types of K-rich volcanic rocks, ranging from lamproite, shoshonite, high-K calc-alkaline basalt-andesite to leucite-bearing silica undersaturated rock (leucitite, melilite, and ugandite), and span a wide range of K_2O contents from 3.6 to 11.2 wt. % and K_2O/Na_2O from 1.1 to 10.4, of which the majority are ultra-potassic (Fig. 1b,c). All samples have trace element patterns

1. Isotope Laboratory, Department of Earth and Space Sciences, University of Washington, Seattle, WA 98195, USA
2. State Key Laboratory of Geological Processes and Mineral Resources, China University of Geosciences, Beijing 100083, China
3. Institute für Geowissenschaften, Johannes Gutenberg Universität, Mainz 55099, Germany
4. Faculty of Mining and Geology, University Belgrade, Đušina 7, Belgrade 11000, Serbia
* Corresponding author (email: zzwang74@uw.edu, fteng@uw.edu)

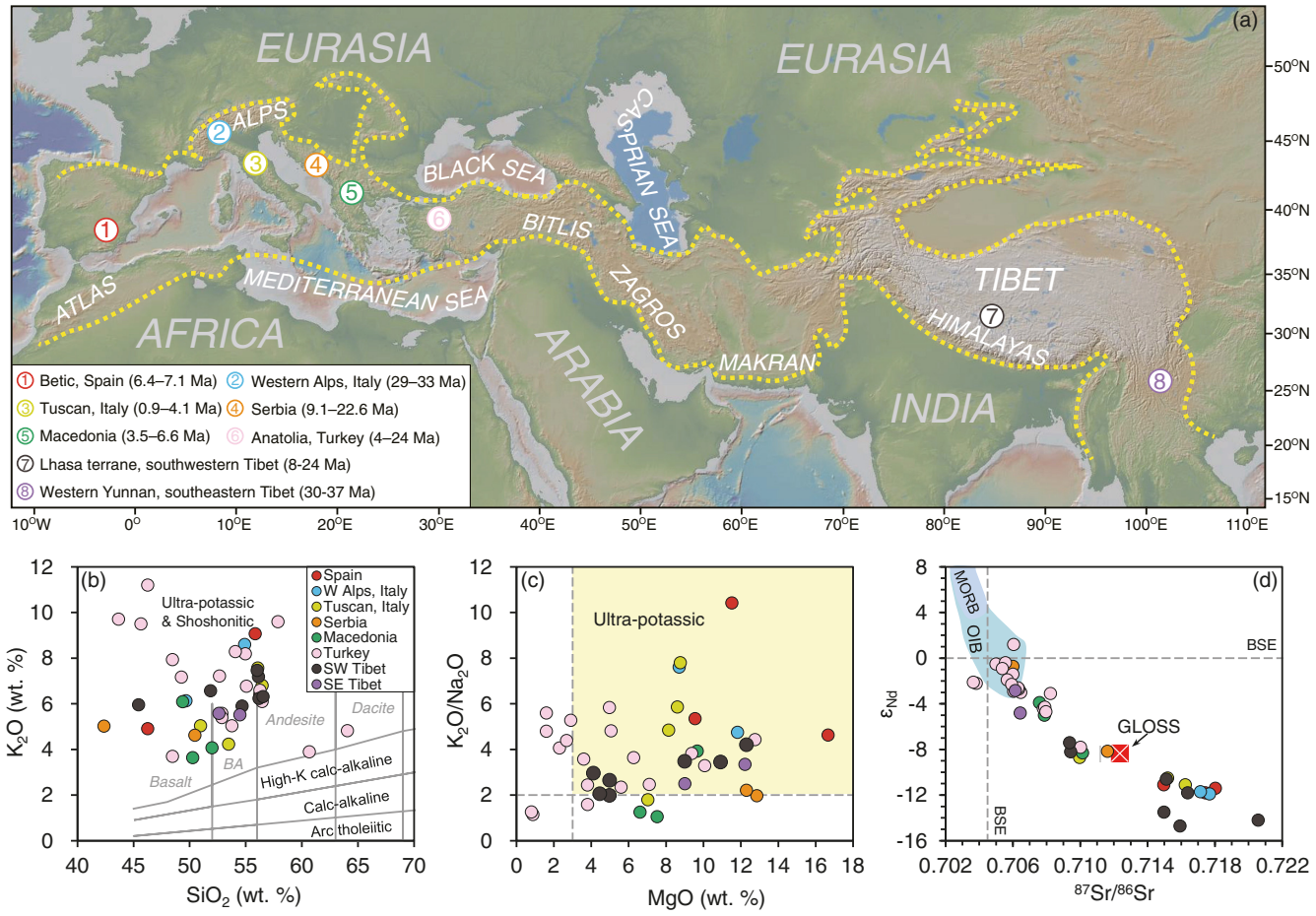

Figure 1 **(a)** Topographic map (http://www.geomapapp.org / CC BY) showing the region of Alpine-Himalayan orogenic belt (bounded by yellow dashed curves). Numbers in circles refer to the locations of K-rich volcanic rocks investigated in this study. **(b)** K_2O *vs.* SiO_2 diagram for classification of volcanic rocks (Peccerillo and Taylor, 1976). **(c)** K_2O/Na_2O *vs.* MgO. The ultra-potassic field is from Foley *et al.* (1987). **(d)** ε_{Nd} *vs.* $^{87}Sr/^{86}Sr$. ε_{Nd} and $^{87}Sr/^{86}Sr$ were calculated at the eruption age. The average global subducting sediments (GLOSS) is from Plank (2014). Major element and Sr-Nd isotope data as well as corresponding references are provided in Table S-1.

resembling upper crustal materials (Fig. S-1) and display a range of Sr and Nd isotopic ratios from OIB-like to continental crust-like (Fig. 1d). Our study finds large K isotopic variation in these K-rich rocks, comparable to subducting sediments, supporting recycling of sediments into the mantle wedge beneath accretionary orogens.

Potassium Isotope Systematics of K-rich Volcanic Rocks

$\delta^{41}K$ of all samples vary from −1.55 ‰ to −0.32 ‰, mimicking the range of global subducting sediments ($\delta^{41}K = -1.30$ ‰ to −0.02 ‰; Hu *et al.*, 2020) (Fig. 2). Two lamproites from Macedonia and Turkey have the lowest $\delta^{41}K$ (−1.55 ± 0.05 ‰ and −0.80 ± 0.05 ‰) reported for mantle-derived lavas. $\delta^{41}K$ of the other 39 samples range from −0.62 ± 0.05 ‰ to −0.32 ± 0.05 ‰, which greatly exceeds our analytical precision (≤0.06 ‰). To date, high precision $\delta^{41}K$ value of the mantle is not well constrained due to the large analytical uncertainties of previous studies (Tuller-Ross *et al.*, 2019a). Nonetheless, the most recent study suggested an average mantle $\delta^{41}K$ of −0.42 ± 0.08 ‰ (2 s.d.; Hu *et al.*, 2021a) and significant numbers of lamproites and shoshonites investigated in this study have resolvably lower $\delta^{41}K$ compared to this mantle value.

Post-eruption alteration processes cannot account for the large K isotopic variation in our samples since correlation between $\delta^{41}K$ and loss on ignition (LOI) is lacking and the isotopically lightest samples have very low LOI (Fig. S-2). Potassium isotope fractionation during partial melting of the

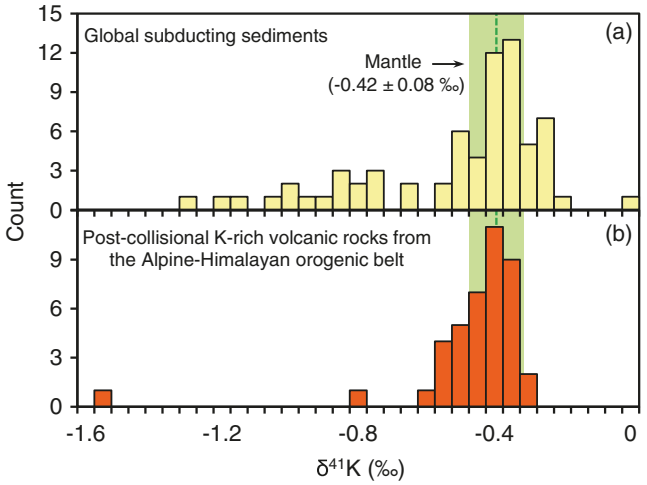

Figure 2 Comparison of $\delta^{41}K$ between global subducting sediments (Hu *et al.*, 2020) and K-rich volcanic rocks from the AHOB (this study). The mantle $\delta^{41}K$ value (−0.42 ± 0.08 ‰) is from Hu *et al.* (2021a).

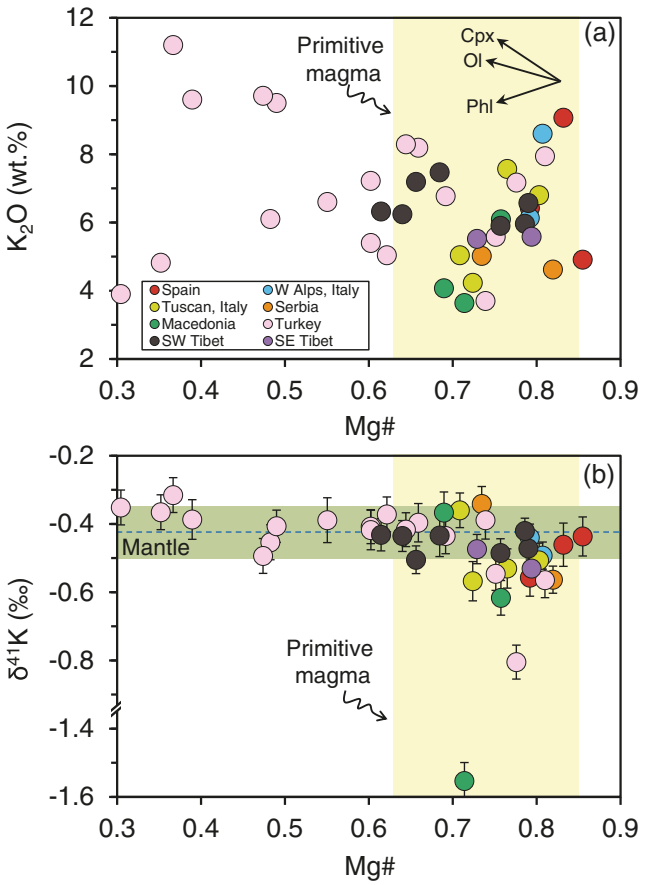

Figure 3 **(a)** K_2O *vs.* Mg#. The vectors qualitatively indicate evolution of melts during fractional crystallisation of olivine (Ol), clinopyroxene (Cpx) and phlogopite (Phl). The yellow bar refers to the putative Mg# range (0.63–0.85) of primitive magmas, which was calculated based on the forsterite contents (85–95 %) of olivine phenocrysts in K-rich volcanic rocks from the AHOB (Prelević *et al.*, 2013) and the experimentally determined olivine-liquid Fe-Mg exchange coefficient ($K_{D,Fe-Mg}^{Ol/liquid} = 0.3$; Roeder and Emslie, 1970). **(b)** $\delta^{41}K$ *vs.* Mg#. The mantle $\delta^{41}K$ (−0.42 ± 0.08 ‰) is from Hu *et al.* (2021a).

mantle and differentiation of mafic magmas is limited and only highly differentiated, Mg-depleted melts have slightly lower $\delta^{41}K$ than primitive melts (Tuller-Ross *et al.*, 2019b; Hu *et al.*, 2021a). The absence of correlation between $\delta^{41}K$ and indices of differentiation such as Mg#, SiO_2 and K_2O in our samples further confirms this (Figs. 3b, S-3). More importantly, low $\delta^{41}K$ values are only observed in samples with Mg# > 0.7 (Fig. 3b), which have been commonly considered as primary or near-primary melts that suffered limited differentiation and crustal contamination (Prelević *et al.*, 2013). Therefore, K isotopic variation in these K-rich lavas most likely reflects source heterogeneity.

Potassium Isotope Heterogeneity in Mantle Sources

Altered oceanic crust (AOC) and sediments dominate the K budget in subducting slabs, which may lead to K isotope heterogeneity in the mantle (Hu *et al.*, 2020). $\delta^{41}K$ of the AOC range from −1.07 ‰ to +0.01 ‰, and hence incorporation of recycled AOC in the mantle can potentially explain the heterogeneous $\delta^{41}K$ in our samples (Hu *et al.*, 2020; Santiago Ramos *et al.*, 2020). However, the AOC is characterised by MORB-like positive ε_{Nd} (Staudigel *et al.*, 1995), inconsistent with the negative ε_{Nd} of the K-rich volcanic rocks (Fig. 1d). Fluids released from subducting oceanic mafic crust were inferred to have higher $\delta^{41}K$ (0.13 ‰ to 1.37 ‰) than the mantle (H. Liu *et al.*, 2020), and hence cannot result in the low $\delta^{41}K$ in our samples. Subducting sediments characterised by variable and negative ε_{Nd} are most likely to be the K source (Fig. 4). Limited K isotope fractionation in subducting sediments occurs during prograde metamorphic dehydration (Wang *et al.*, 2021). Therefore, K isotopic signatures of subducting sediments could be transferred to the mantle source of K-rich lavas.

Heavy K isotopes were preferentially released into hydrosphere during continental weathering, leaving the residues enriched in light K isotopes (Li *et al.*, 2019; Chen *et al.*, 2020; Teng *et al.*, 2020). Terrigenous sediments that underwent moderate to intensive weathering display a range of $\delta^{41}K$ from −0.70 ‰ to −0.35 ‰ (Hu *et al.*, 2020), covering $\delta^{41}K$ of all but two of our samples. Incorporation of K into authigenic clay minerals during diagenesis strongly favours light K isotopes, producing sediments with $\delta^{41}K$ down to −1.31 ‰ (Hu *et al.*, 2020), which approaches the lowest value of our samples. Therefore, recycled authigenic clay-rich sediments, which are difficult to identify by trace elements and radiogenic isotopes, likely contribute to K in the two lamproites with extremely low $\delta^{41}K$. The scarcity of such samples is also consistent with the low fractions of isotopically light clay-rich sediments in global subducting sediments (Fig. 2). In addition, these low $\delta^{41}K$ lamproites mainly occur in the eastern Mediterranean provinces (Serbia, Macedonia, and Turkey) and are characterised by less radiogenic Sr and unradiogenic Nd isotopic signatures compared to the western Mediterranean counterparts (Spain and Italy), which reflects involvement of sediments with different age and provenance in their sources (Prelević *et al.*, 2008). The distinct K isotopic feature between samples from these two provinces further indicates regional heterogeneity in $\delta^{41}K$ of recycled sediments.

A Monte Carlo mixing model between the DMM (depleted MORB mantle) and subducted sediments shows that the addition of up to 5 % sediment in the mantle can almost reproduce the full range of $\delta^{41}K$ in these K-rich volcanic rocks

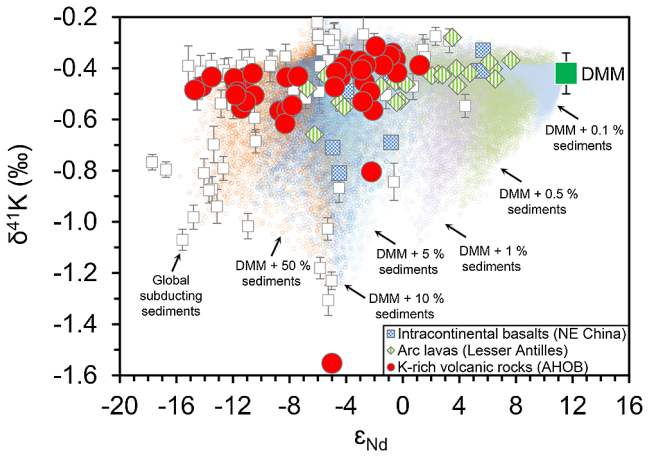

Figure 4 $\delta^{41}K$ *vs.* ε_{Nd} (calculated back at the eruption or depositional age). The $\delta^{41}K$ and ε_{Nd} of global subducting sediments are from Hu *et al.* (2020) and Plank (2014). $\delta^{41}K$ of the DMM is assumed to be the average mantle value and ε_{Nd} of the DMM is from Workman and Hart (2005). Small circles with different colours represent random mixing of subducted sediments with the DMM at variable proportions from a Monte Carlo simulation, of which the details are provided in the Supplementary Information.

because of the much higher K content in sediments than in the mantle (Fig. 4). The actual amount of sediment may be much lower considering that sediment melts, which are more enriched in incompatible elements than bulk sediments, were most likely added into the mantle. The sediment fraction derived above is significantly lower than that used in partial melting experiments on a mixture of peridotite and sediment or sediment-derived melt to generate ultra-potassic melts (≥25 %; Mallik *et al.*, 2015; Förster *et al.*, 2020). Therefore, if the experimental amount of sediment is employed in our model, $\delta^{41}K$ of ultra-potassic melts will completely inherit those of recycled sediments. Overall, recycling of a small amount of isotopically anomalous sediments into the mantle can significantly modify $\delta^{41}K$ of the mantle. This process can adequately explain the large variations of $\delta^{41}K$ and especially low $\delta^{41}K$ that are often observed in isotopically "enriched" (*i.e.* low ε_{Nd}) mantle-derived melts erupted in various tectonic settings (Fig. 4). Therefore, K isotopes may become one of the most sensitive indicators for the presence of sediments in the mantle.

Acknowledgements

We are grateful to Xin-Yang Chen, Yan Hu, Tian-Yi Huang, Pete Wynn and Kai-Chen Xing for their help during K isotopic analysis. Constructive comments from Dr. Oscar Laurent, one anonymous reviewer and the editor Dr. Maud Boyet are highly appreciated. This work is financially supported by the National Key R&D Program of China (2019YFA0708400) and the Programme of Introducing Talents of Discipline to Universities (*i.e.* the 111 project; B18048) to S.-A. Liu.

Editor: Maud Boyet

Additional Information

Supplementary Information accompanies this letter at https://www.geochemicalperspectivesletters.org/article2123.

Cite this letter as: Wang, Z.-Z., Teng, F.-Z., Prelević, D., Liu, S.-A., Zhao, Z. (2021) Potassium isotope evidence for sediment recycling into the orogenic lithospheric mantle. *Geochem. Persp. Let.* 18, 43–47.

References

Avanzinelli, R., Lustrino, M., Mattei, M., Melluso, L., Conticelli, S. (2009) Potassic and ultrapotassic magmatism in the circum-Tyrrhenian region: significance of carbonated pelitic vs. pelitic sediment recycling at destructive plate margins. *Lithos* 113, 213–227.

Chen, H., Liu, X.-M., Wang, K. (2020) Potassium isotope fractionation during chemical weathering of basalts. *Earth and Planetary Science Letters* 539, 116192.

Conticelli, S., Guarnieri, L., Farinelli, A., Mattei, M., Avanzinelli, R., Bianchini, G., Boari, E., Tommasini, S., Tiepolo, M., Prelević, D. (2009) Trace elements and Sr–Nd–Pb isotopes of K-rich, shoshonitic, and calc-alkaline magmatism of the Western Mediterranean Region: genesis of ultrapotassic to calc-alkaline magmatic associations in a post-collisional geodynamic setting. *Lithos* 107, 68–92.

Couzinié, S., Laurent, O., Moyen, J.-F., Zeh, A., Bouilhol, P., Villaros, A. (2016) Post-collisional magmatism: crustal growth not identified by zircon Hf–O isotopes. *Earth and Planetary Science Letters* 456, 182–195.

Foley, S., Venturelli, G., Green, D., Toscani, L. (1987) The ultrapotassic rocks: characteristics, classification, and constraints for petrogenetic models. *Earth-Science Reviews* 24, 81–134.

Förster, M.W., Buhre, S., Xu, B., Prelević, D., Mertz-Kraus, R., Foley, S.F. (2020) Two-stage origin of K-enrichment in ultrapotassic magmatism simulated by melting of experimentally metasomatized mantle. *Minerals* 10, 41.

Hu, Y., Teng, F.-Z., Plank, T., Chauvel, C. (2020) Potassium isotopic heterogeneity in subducting oceanic plates. *Science Advances* 6, eabb2472.

Hu, Y., Teng, F.Z., Helz, R.T., Chauvel, C. (2021a) Potassium isotope fractionation during magmatic differentiation and the composition of the mantle. *Journal of Geophysical Research: Solid Earth* 126, e2020JB021543.

Hu, Y., Teng, F.-Z., Chauvel, C. (2021b) Potassium isotopic evidence for sedimentary input to the mantle source of Lesser Antilles lavas. *Geochimica et Cosmochimica Acta* 295, 98–111.

Huang, T.-Y., Teng, F.-Z., Rudnick, R.L., Chen, X.-Y., Hu, Y., Liu, Y.-S., Wu, F.-Y. (2020) Heterogeneous potassium isotopic composition of the upper continental crust. *Geochimica et Cosmochimica Acta* 278, 122–136.

Li, S., Li, W., Beard, B.L., Raymo, M.E., Wang, X., Chen, Y., Chen, J. (2019) K isotopes as a tracer for continental weathering and geological K cycling. *Proceedings of the National Academy of Sciences* 116, 8740–8745.

Liu, H., Wang, K., Sun, W.-D., Xiao, Y., Xue, Y.-Y., Tuller-Ross, B. (2020) Extremely light K in subducted low-T altered oceanic crust: Implications for K recycling in subduction zone. *Geochimica et Cosmochimica Acta* 277, 206–223.

Liu, S.A., Wang, Z.Z., Yang, C., Li, S.G., Ke, S. (2020) Mg and Zn isotope evidence for two types of mantle metasomatism and deep recycling of magnesium carbonates. *Journal of Geophysical Research: Solid Earth*, e2020JB020684.

Mallik, A., Nelson, J., Dasgupta, R. (2015) Partial melting of fertile peridotite fluxed by hydrous rhyolitic melt at 2–3 GPa: implications for mantle wedge hybridization by sediment melt and generation of ultrapotassic magmas in convergent margins. *Contributions to Mineralogy and Petrology* 169, 48.

Peccerillo, A., Taylor, S. (1976) Geochemistry of Eocene calc-alkaline volcanic rocks from the Kastamonu area, northern Turkey. *Contributions to Mineralogy and Petrology* 58, 63–81.

Plank, T. (2014) 4.17 – The chemical composition of subducting sediments. In: Holland, H.D., Turekian, K.K. (Eds.) *Treatise on Geochemistry*. Second Edition, Elsevier, Oxford, 607–629.

Prelević, D., Foley, S.F., Romer, R.L., Cvetković, V., Downes, H. (2005) Tertiary ultrapotassic volcanism in Serbia: constraints on petrogenesis and mantle source characteristics. *Journal of Petrology* 46, 1443–1487.

Prelević, D., Foley, S.F., Romer, R., Conticelli, S. (2008) Mediterranean Tertiary lamproites derived from multiple source components in postcollisional geodynamics. *Geochimica et Cosmochimica Acta* 72, 2125–2156.

Prelević, D., Akal, C., Foley, S.F., Romer, R.L., Stracke, A., Van Den Bogaard, P. (2012) Ultrapotassic mafic rocks as geochemical proxies for post-collisional dynamics of orogenic lithospheric mantle: the case of southwestern Anatolia, Turkey. *Journal of Petrology* 53, 1019–1055.

Prelević, D., Jacob, D.E., Foley, S.F. (2013) Recycling plus: a new recipe for the formation of Alpine–Himalayan orogenic mantle lithosphere. *Earth and Planetary Science Letters* 362, 187–197.

Prelević, D., Akal, C., Romer, R.L., Mertz-Kraus, R., Helvaci, C. (2015) Magmatic response to slab tearing: constraints from the Afyon Alkaline Volcanic Complex, Western Turkey. *Journal of Petrology* 56, 527–562.

Roeder, P.L., Emslie, R. (1970) Olivine-liquid equilibrium. *Contributions to Mineralogy and Petrology* 29, 275–289.

Santiago Ramos, D.P., Coogan, L.A., Murphy, J.G., Higgins, J.A. (2020) Low-temperature oceanic crust alteration and the isotopic budgets of potassium and magnesium in seawater. *Earth and Planetary Science Letters* 541, 116290.

Staudigel, H., Davies, G.R., Hart, S.R., Marchant, K.M., Smith, B.M. (1995) Large scale isotopic Sr, Nd and O isotopic anatomy of altered oceanic crust: DSDP/ODP sites 417/418. *Earth and Planetary Science Letters* 130, 169–185.

Sun, Y., Teng, F.-Z., Hu, Y., Chen, X.-Y., Pang, K.-N. (2020) Tracing subducted oceanic slabs in the mantle by using potassium isotopes. *Geochimica et Cosmochimica Acta* 278, 353–360.

Teng, F.-Z., Hu, Y., Ma, J.-L., Wei, G.-J., Rudnick, R.L. (2020) Potassium isotope fractionation during continental weathering and implications for global K isotopic balance. *Geochimica et Cosmochimica Acta* 278, 261–271.

Tommasini, S., Avanzinelli, R., Conticelli, S. (2011) The Th/La and Sm/La conundrum of the Tethyan realm lamproites. *Earth and Planetary Science Letters* 301, 469–478.

Tuller-Ross, B., Marty, B., Chen, H., Kelley, K.A., Lee, H., Wang, K. (2019a) Potassium isotope systematics of oceanic basalts. *Geochimica et Cosmochimica Acta* 259, 144–154.

Tuller-Ross, B., Savage, P.S., Chen, H., Wang, K. (2019b) Potassium isotope fractionation during magmatic differentiation of basalt to rhyolite. *Chemical Geology* 525, 37–45.

Walter, M.J. (1998) Melting of garnet peridotite and the origin of komatiite and depleted lithosphere. *Journal of Petrology* 39, 29–60.

Wang, Z.-Z, Teng, F.-Z., Busigny, V., Liu, S.-A. (2021) Evidence from HP/UHP metasediments for subduction of isotopically heterogeneous potassium into the mantle. *American Mineralogist* in press. doi: 10.2138/am-2021-7923.

Williams, H.M., Turner, S.P., Pearce, J.A., Kelley, S., Harris, N. (2004) Nature of the source regions for post-collisional, potassic magmatism in southern and northern Tibet from geochemical variations and inverse trace element modelling. *Journal of Petrology* 45, 555–607.

Workman, R.K., Hart, S.R. (2005) Major and trace element composition of the depleted MORB mantle (DMM). *Earth and Planetary Science Letters* 231, 53–72.

Zhao, Z., Mo, X., Dilek, Y., Niu, Y., DePaolo, D.J., Robinson, P., Zhu, D., Sun, C., Dong, G., Zhou, S. (2009) Geochemical and Sr–Nd–Pb–O isotopic compositions of the post-collisional ultrapotassic magmatism in SW Tibet: petrogenesis and implications for India intra-continental subduction beneath southern Tibet. *Lithos* 113, 190–212.

Geochemical Perspectives Letters

Potassium isotope evidence for sediment recycling into the orogenic lithospheric mantle

Z.-Z. Wang, F.-Z. Teng, D. Prelević, S.-A. Liu, Z. Zhao

Supplementary Information

The Supplementary Information includes:

- 1. Sample Description and Petrogenesis of Samples Investigated in This Study
- 2. Analytical Method
- 3. Monte Carlo Isotope Mixing Model
- Table S-1
- Figures S-1 to S-3
- Supplementary Information References

1. Sample Description and Petrogenesis of Samples Investigated in This Study

1.1. Western Mediterranean provinces

Nine samples from Spain and Italy are from this area. Their lithologies are lamproites but two shoshonites from the Tuscan volcanic province, Italy. Potassic volcanism in this area lasted from the Oligocene (29–33 Ma at western Alps, Italy) to the Pleistocene (0.9–4.1 Ma at Tuscan, Italy) and mainly occurred in a collisional suture that originated during south-eastward subduction of the Jurassic Alpine (Piemont–Ligurian) ocean beneath African plate with Hercynian Europe acting as a passive margin (Prelević *et al.*, 2008). They are characterised by extremely high $^{87}Sr/^{86}Sr$ (0.70997 to 0.71803) and low ε_{Nd} (−11.9 to −8.7) (Fig. 1d). These signatures indicate that these lavas were produced by partial melting of a heavily metasomatised lithospheric mantle source during post-collisional tectonics. Three components were suggested to contribute to the formation of these lavas, that is, (1) an ultra-depleted mantle component probably originating from an island-arc-oceanic lithospheric block, accreted during Alpine collisional processes to the older lithospheric domains, (2) a Hercynian crustal component, and (3) a convecting mantle component defined as European asthenospheric reservoir, which has been taken as the source of European Cenozoic sodic volcanism (Prelević *et al.*, 2008 and references therein).

1.2. Eastern Mediterranean provinces

Samples from this area include: one Early Miocene (22.6 Ma) lamproite and one Late Miocene (9.12 Ma) ugandite from Serbia (Prelević *et al.*, 2005); three Pliocene (2–3.8 Ma) lamproites from Macedonia (Prelević *et al.*, 2008); nine Miocene–Pliocene (4.7–11.8 Ma) lamproites from the southwestern Anatolia, Turkey (Prelević *et al.*, 2012); nine Miocene (11.4 Ma) alkaline volcanic complex samples including shoshonite, latite, (melilite-) leucitite and tephriphonolite from the Miocene Afyon volcanic province, western Turkey (Prelević *et al.*, 2015). In general, the K-rich lavas from this area can be classified into two groups: (1) ultrapotassic, shoshonitic, and high-K calc-alkaline group and (2) kamfugitic group, which is represented by the Serbian ugandite and Turkey melilite-leucitite. The group 1 rocks are silica-saturated, while the group 2 rocks are silica-undersaturated and leucite-bearing. Similar to the lamproites from the western Mediterranean provinces, the group 1 rocks were also suggested to derive from a lithospheric mantle source that underwent at least two episodes of metasomatism: the first-stage mantle metasomatism involved melts derived from subducted sediments; the second-stage metsomatic agent was ultimately derived from the asthenosphere. Compared to the western Mediterranean counterparts, the group 1 samples from the eastern Mediterranean provinces have less radiogenic Sr and unradiogenic Nd isotopic compositions (Fig. 1d). These radiogenic isotopic signatures indicate that the sediments incorporated into their mantle sources are from younger crust, which are probably derived from the north African continent and mixed with other oceanic sediments from the top of the accreting oceanic lithosphere and/or subduction zone mélange (Prelević *et al.*, 2008; 2012). The group 2 rocks were considered as products of melting of phlogopite-wehrlite metasomes, which were likely formed by infiltration of carbonatitic components into the lithospheric mantle (Prelević *et al.*, 2015). In addition, the Turkey melilite-leucitites have experienced extreme clinopyroxene fractionation combined with leucite accumulation, resulting in the low Mg# of these samples (Prelević *et al.*, 2015) (Fig. 3).

1.3. Tibet

The Tibetan samples contain seven Miocene (8–24 Ma) (basaltic) trachyandesites from the Lhasa terrain, southwestern Tibet (Zhao *et al.*, 2009; Liu *et al.*, 2015) and three Late Eocene (36 Ma) shoshonites from western Yunnan, southeastern Tibet (Liu *et al.*, 2020). Samples from Lhasa terrain have extremely variable and high $^{87}Sr/^{86}Sr$ (0.70938 to 0.72057) and low ε_{Nd} (−14.7 to −7.4), while the western Yunnan samples have more restricted and lower $^{87}Sr/^{86}Sr$ (0.70615 to 0.70644) and higher ε_{Nd} (−2.8 to −4.8). The Lhasa ultrapotassic lavas were suggested to be formed by partial melting of an upper mantle reservoir metasomatised by materials derived from the subducted Indian continents (Zhao *et al.*, 2009). The sources of the western Yunnan shoshonites were considered to be a metasomatised lithospheric mantle modified by sediment-derived fluids or melts related to the Proterozoic and Palaeozoic subduction beneath the western part of the Yangtze craton, China (Guo *et al.*, 2005).

2. Analytical Method

Potassium isotopic analysis was performed following previous methods (Hu *et al.*, 2018; Xu *et al.*, 2019) at the Isotope Laboratory of the University of Washington, Seattle. Around 5 to 10 mg whole-rock powders were digested in an acid mixture of Optima-grade HF-HNO_3-HCl. After complete dissolution, the solution was dried down and redissolved in 1 ml 0.5 N HNO_3 in preparation for chromatographic purification. Potassium was separated from matrix elements using AG 50W-X8 cation exchange resin (200–400 mesh). The recovery of K is over 99 % and the total procedural blank contains less than 9 ng of K, which accounts for negligible portion (<0.1 %) of the loaded K.

A Nu Plasma II multicollector inductively coupled plasma mass spectrometer (MC-ICP-MS) was used for K isotopic measurement. In order to suppress the interferences from argon hydrides (*e.g.*, $Ar^{38}H^+$ and $Ar^{40}H^+$), we introduced samples into the plasma via a CETAC Aridus II desolvating nebuliser system, and reduced the RF power to 700 W. The peaks of $^{39}K^+$ and $^{41}K^+$ were monitored simultaneously at the left shoulder without interferences in a pseudo-high resolution mode ($M/\Delta M$ = ~10,000). Around 4 to 6 V signals of $^{39}K^+$ for a 10^{11} Ω resistor is routinely obtained for a solution of 3 ppm K. Instrumental mass bias correction was achieved by standard-sample bracketing method. The results are reported in conventional δ notation relative to the NIST K standard SRM 3141a:

$$\delta^{41}\mathrm{K}\ (‰) = \left\{ \frac{\left(^{41}\mathrm{K}/^{39}\mathrm{K}\right)_{\mathrm{sample}}}{\left(^{41}\mathrm{K}/^{39}\mathrm{K}\right)_{\mathrm{SRM\ 3141a}}} - 1 \right\} \times 1000$$

An external uncertainty in $\delta^{41}K$ better than 0.06 ‰ (95 % confidential interval) was obtained by repeat analyses of rock standards and synthetic K solutions over a period of two years (Hu *et al.*, 2018; Xu *et al.*, 2019). Four igneous standards AGV-1, BCR-1, JB-1 and DR-N were analysed together with unknown samples to assess the accuracy in this study and their results agree well with the published values (Morgan *et al.*, 2018; Chen *et al.*, 2019; Xu *et al.*, 2019; Li *et al.*, 2020).

3. Monte Carlo Isotope Mixing Model

The K_2O content and K isotopic composition of sediment-mantle mixture can be calculated using the following mass balance equations:

$$[K_2O]_{mix} = [K_2O]_{sediment} \times F + [K_2O]_{mantle} \times (1 - F) \quad (1)$$

$$[K_2O]_{mix} \times \delta^{41}K_{mix} = [K_2O]_{sediment} \times \delta^{41}K_{sediment} \times F + [K_2O]_{mantle} \times \delta^{41}K_{mantle} \times (1 - F) \quad (2)$$

F refers to the sediment mass flux into the mantle.

Likewise, the Nd concentration and ε_{Nd} value of sediment-mantle mixture can also be obtained. To explore the composition range of sediments under as many as possible scenarios, we randomly selected three sediments from the global subducting sediment database (Hu *et al.*, 2020) and then they were mixed at random proportions to make a new sediment endmember. Finally, this new sediment was mixed with the mantle at a sediment proportion of 0.1 %, 0.5 %, 1 %, 5 %, 10 %, and 50 %, respectively. A total of 10,000 sediment-mantle mixtures were yielded using this method. The modelling results are shown in Figure 4.

Supplementary Table

Table S-1 Potassium isotopic compositions of K-rich volcanic rocks from the Alpine-Himalayan orogenic belt and geostandards, along with sample location, lithology, age, and selected element and Sr-Nd isotope data.

Sample	Ref.	Location	Lithology	Age (Ma)	SiO_2 (wt. %)	MgO (wt. %)	Na_2O (wt. %)	K_2O (wt. %)	LOI (wt. %)	Mg#	$^{87}Sr/^{86}Sr$	ε_{Nd}	$\delta^{41}K$ (‰)	2 s.d. (‰)	95 % c.i. (‰)	*N*
03J10	1	Spain	Lamproite	6.8	46.2	16.66	1.06	4.91	4.15	0.85	0.71497	−11.1	−0.44	0.06	0.06	7
Replicate													−0.42	0.08	0.05	13
Replicate													−0.40	0.07	0.07	6
02CX05	1	Spain	Lamproite	7	55.77	11.51	0.87	9.07	0.68	0.83	0.71744	−11.8	−0.46	0.07	0.06	6
Replicate													−0.48	0.08	0.06	13
03FC01	1	Spain	Lamproite	7.1	56.19	9.55	1.2	6.42	3.62	0.79	0.71803	−11.4	−0.56	0.09	0.05	14
05RR02	1	Western Alps	Lamproite	30	49.61	11.82	1.29	6.13	1.26	0.79	0.71769	−11.9	−0.44	0.05	0.04	7
05VDA03	1	Western Alps	Lamproite	30	54.83	8.7	1.13	8.6	3.27	0.81	0.71714	−11.7	−0.49	0.06	0.04	7
Replicate													−0.45	0.07	0.05	13
VUL 9703A	2	Tuscan, Italy	Shoshonite	0.9–4.1	53.4	7.02	2.35	4.23	1.02	0.72	0.70997	−8.7	−0.57	0.07	0.06	6
ORC 9702	2	Tuscan, Italy	Lamproite	0.9–4.1	56.4	8.6	1.16	6.8	4.99	0.80	0.7152	−10.5	−0.51	0.06	0.05	7
AMT 9703 II	2	Tuscan, Italy	Shoshonite	0.9–4.1	50.9	8.13	1.04	5.04	1.4	0.71			−0.36	0.09	0.05	7
TA 9701	2	Tuscan, Italy	Lamproite	0.9–4.1	56	8.76	0.97	7.57	0.51	0.76	0.71625	−11.1	−0.53	0.09	0.06	6
BK01/3-1	3	Serbia	Lamproite	22.6	50.4	12.85	2.34	4.62	3.77	0.82	0.71162	−8.2	−0.56	0.06	0.04	7
KR01/1	3	Serbia	Ugandite	9.12	42.3	12.29	2.27	5.02	1.95	0.73	0.706	−0.7	−0.34	0.07	0.05	14
Replicate													−0.32	0.08	0.05	13
04CR01	1	Macedonia	Lamproite	3.5	51.92	6.6	3.24	4.07	1.92	0.69	0.70759	−3.9	−0.37	0.06	0.06	12
04SL01	1	Macedonia	Lamproite	3.8	50.2	7.52	3.44	3.64	1.07	0.71	0.70788	−5	−1.55	0.09	0.05	14
Replicate													−1.51	0.08	0.06	7

Table S-1 continued

Sample	Ref.	Location	Lithology	Age (Ma)	SiO_2 (wt. %)	MgO (wt. %)	Na_2O (wt. %)	K_2O (wt. %)	LOI (wt. %)	Mg#	$^{87}Sr/^{86}Sr$	ε_{Nd}	$\delta^{41}K$ (‰)	2 s.d. (‰)	95 % c.i. (‰)	*N*
03KK04	1	Macedonia	Lamproite	2	49.31	9.66	1.55	6.09	2.6	0.76	0.71014	−8.3	−0.62	0.07	0.05	14
Replicate													−0.60	0.09	0.06	7
Replicate													−0.57	0.07	0.06	13
05KD03	4	Turkey	Lamproite	11.8	53.7	5.59	2.15	5.04	1.06	0.62	0.70647	−3	−0.37	0.07	0.05	7
05KD14	4	Turkey	Lamproite	11.8	64	0.88	4.2	4.82	0.23	0.35	0.705	−0.5	−0.37	0.05	0.05	7
06KD21	4	Turkey	Lamproite	11.8	55	6.26	1.86	6.77	1.25	0.69	0.70781	−4.4	−0.44	0.09	0.05	14
05GU02	4	Turkey	Lamproite	15.5	52.8	9.37	1.46	5.58	3.38	0.75	0.71002	−7.8	−0.55	0.06	0.05	7
06KZ01	4	Turkey	Lamproite	18.6	52.6	3.59	2.02	7.22	5.62	0.6	0.70824	−3.1	−0.41	0.07	0.05	7
05IL01	4	Turkey	Lamproite	11.9	54.9	5.06	1.7	8.19	1.76	0.66	0.7079	−4.3	−0.40	0.08	0.06	13
05BH05	4	Turkey	Lamproite	11.4	54	4.97	1.42	8.29	5.94	0.64	0.70796	−4.7	−0.42	0.05	0.05	7
05BSS02	4	Turkey	Lamproite	4.5	49.2	10.06	2.18	7.17	1.32	0.78	0.70383	−2.2	−0.80	0.05	0.05	7
Replicate													−0.78	0.08	0.06	7
06BSS14	4	Turkey	Lamproite	4.7	48.4	12.75	1.79	7.94	1.32	0.81	0.70366	−2.1	−0.56	0.10	0.05	12
Replicate													−0.53	0.09	0.06	12
06AF03	4	Turkey	Leucitite	11.4	43.6	2.68	2.21	9.71	5.97	0.47	0.70593	−2.3	−0.49	0.05	0.05	7
31	5	Turkey	Shoshonite	11.4	52.8	3.8	3.4	5.4	2.1	0.60	0.70556	−0.4	−0.42	0.08	0.06	6
84	5	Turkey	Latite	11.4	60.6	0.8	3.1	3.9	0.9	0.30	0.70538	−0.9	−0.35	0.08	0.05	7
60	5	Turkey	Phonotephrite	11.4	48.4	7.1	1.5	3.7	0.4	0.74	0.70605	1.2	−0.39	0.08	0.06	6
50	5	Turkey	Latite	11.4	56.2	3.8	2.7	6.6	0.5	0.55	0.70601	−1.4	−0.39	0.07	0.07	5
42	5	Turkey	Tephriphonolite	11.4	56.4	2.3	1.5	6.1	1.1	0.48	0.70635	−2.7	−0.45	0.10	0.05	7
23/A	5	Turkey	Tephriphonolite	11.4	57.8	1.6	2	9.6	1.3	0.39	0.70631	−2.6	−0.39	0.06	0.06	6
1/A	5	Turkey	Melilite leucitite	11.4	46.2	1.6	2	11.2	2.6	0.37	0.70567	−1.9	−0.32	0.05	0.05	7
19/A	5	Turkey	Melilite leucitite	11.4	45.6	2.9	1.8	9.5	4	0.49	0.70605	−2.9	−0.41	0.09	0.05	14
Replicate													−0.40	0.08	0.05	13

Table S-1 continued

Sample	Ref.	Location	Lithology	Age (Ma)	SiO_2 (wt. %)	MgO (wt. %)	Na_2O (wt. %)	K_2O (wt. %)	LOI (wt. %)	Mg#	$^{87}Sr/^{86}Sr$	ε_{Nd}	$\delta^{41}K$ (‰)	2 s.d. (‰)	95 % c.i. (‰)	*N*
CQ01	6	SW Tibet	Basaltic trachyandesite	8–24	51.79	10.92	1.91	6.57	0.54	0.79	0.72057	−14.2	−0.47	0.05	0.04	12
Replicate													−0.45	0.05	0.05	7
D9103	6	SW Tibet	Trachyandesite	8–24	56.07	4.99	2.72	7.19	0.9	0.66	0.71638	−11.8	−0.51	0.05	0.04	14
GGP-7	6	SW Tibet	Tephrite	8–24	45.39	12.3	1.42	5.96	1.81	0.79	0.71512	−10.6	−0.42	0.10	0.04	6
Z8030-5	6	SW Tibet	Trachyte	8–24	55.96	4.12	2.53	7.47	2.95	0.68	0.71498	−13.5	−0.43	0.06	0.06	14
ZB3	6	SW Tibet	Trachyandesite	8–25	56.12	4.98	3.15	6.24	0.39	0.64	0.70943	−8.2	−0.44	0.06	0.05	6
ZB10	6	SW Tibet	Trachyandesite	8–26	56.48	4.46	3.08	6.32	0.64	0.61	0.70938	−7.4	−0.43	0.08	0.05	6
SL0621	6	SW Tibet	Trachyandesite	8–27	54.6	9.00	1.70	5.90	0.70	0.76	0.71594	−14.7	−0.49	0.05	0.04	7
Replicate													−0.49	0.08	0.05	14
HZ06	7	SE Tibet	Shoshonite	36	54.41	9.00	2.21	5.52	0.87	0.73	0.70644	−4.8	−0.47	0.07	0.04	14
HZ13	7	SE Tibet	Shoshonite	36	52.54	12.21	1.67	5.58	0.89	0.79	0.70615	−2.8	−0.53	0.05	0.04	14
Replicate													−0.52	0.08	0.07	6
Geostandards																
AGV-1													−0.44	0.04	0.03	7
BCR-1													−0.40	0.08	0.04	7
JB-1													−0.44	0.09	0.05	6
DR-N													−0.54	0.08	0.06	14

Notes: Mg# = molar ratio of Mg/(Mg + 0.85*total Fe). 2 s.d. and 95 % c.i. refer to two standard deviation and 95 % confidential interval of *N* repeated measurements on the same sample solution, respectively. Replicate represents repeated dissolution, column chemistry and spectrometric analysis. Age, major element, and Sr-Nd isotope data are from: 1, Prelević *et al.*, 2008; 2, Barnekow, 2000; 3, Prelević *et al.*, 2005; 4, Prelević *et al.*, 2012; 5, Prelević *et al.*, 2015; 6, Zhao *et al.*, 2009; 7, Liu *et al.*, 2020.

Supplementary Figures

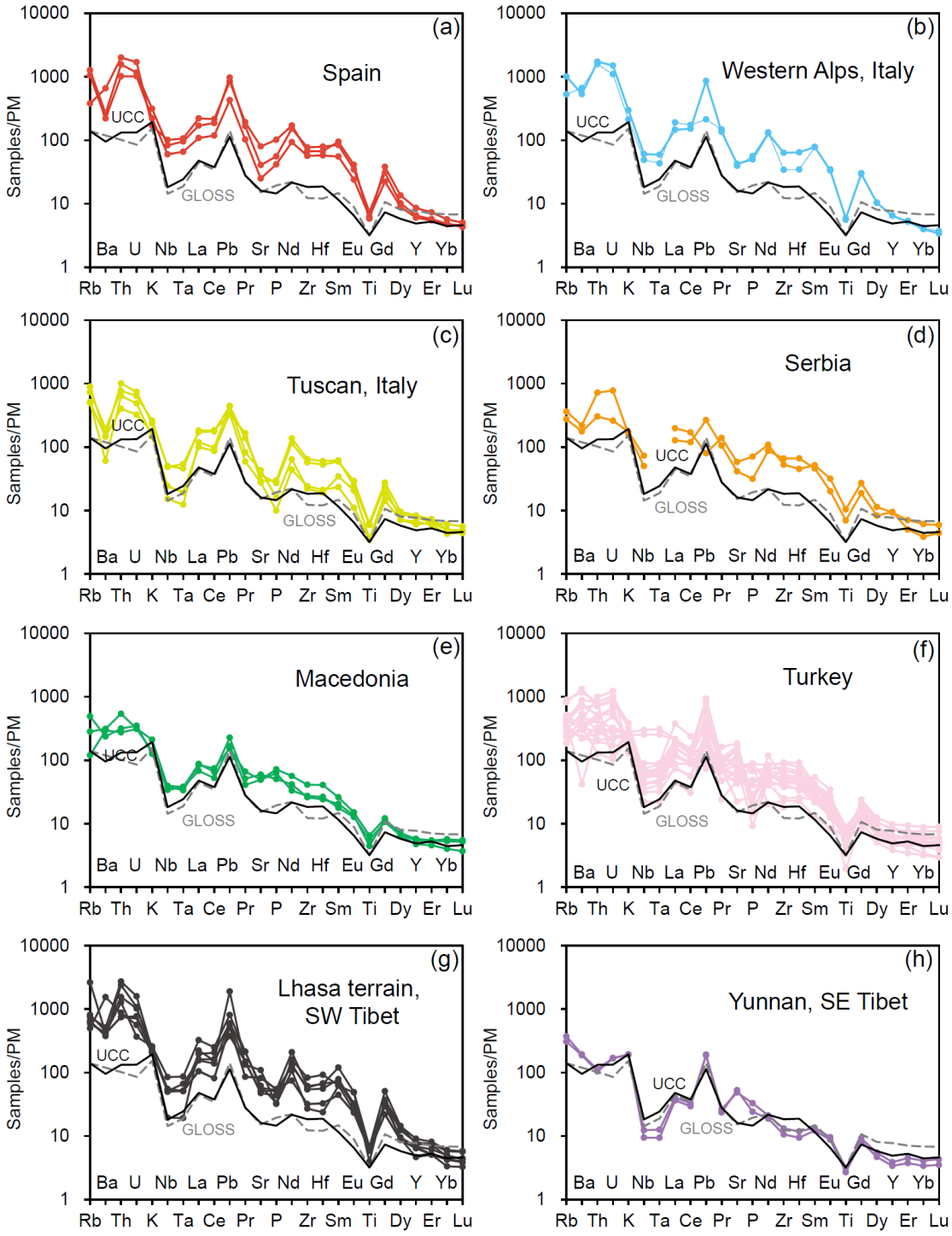

Figure S-1 Primitive mantle (PM)-normalised trace element patterns for the K-rich volcanic rocks investigated in this study. The PM values for normalisation are from Mcdonough and Sun (1995). The compositions of global subducting sediment (GLOSS) and upper continental crust (UCC) are plotted for comparison (Plank, 2014; Rudnick and Gao, 2014).

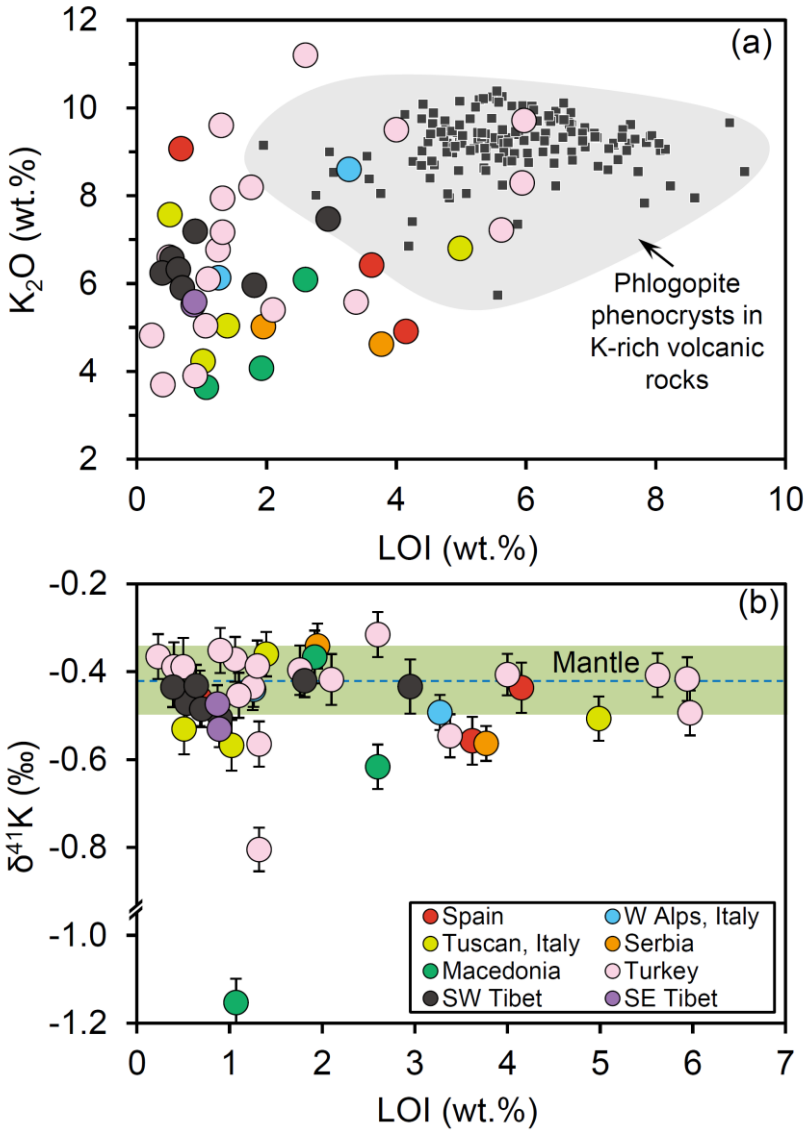

Figure S-2 **(a)** K_2O vs. loss on ignition (LOI). Data for phlogopite phenocrysts in K-rich volcanic rocks from the AHOB are plotted for comparison (Zhao *et al.*, 2009; Prelević *et al.*, 2005, 2012). **(b)** $\delta^{41}K$ vs. LOI. A few samples have high loss on ignition (LOI) contents, which primarily reflects the enrichment of hydrous K-rich minerals, as indicated by the roughly positive trend between LOI and K_2O towards phlogopite phenocrysts. Besides, no correlation between $\delta^{41}K$ and LOI is observed and the isotopically lightest samples have very low LOI. Therefore, post-eruption alteration processes are unlikely to account for the K isotopic variation in our samples.

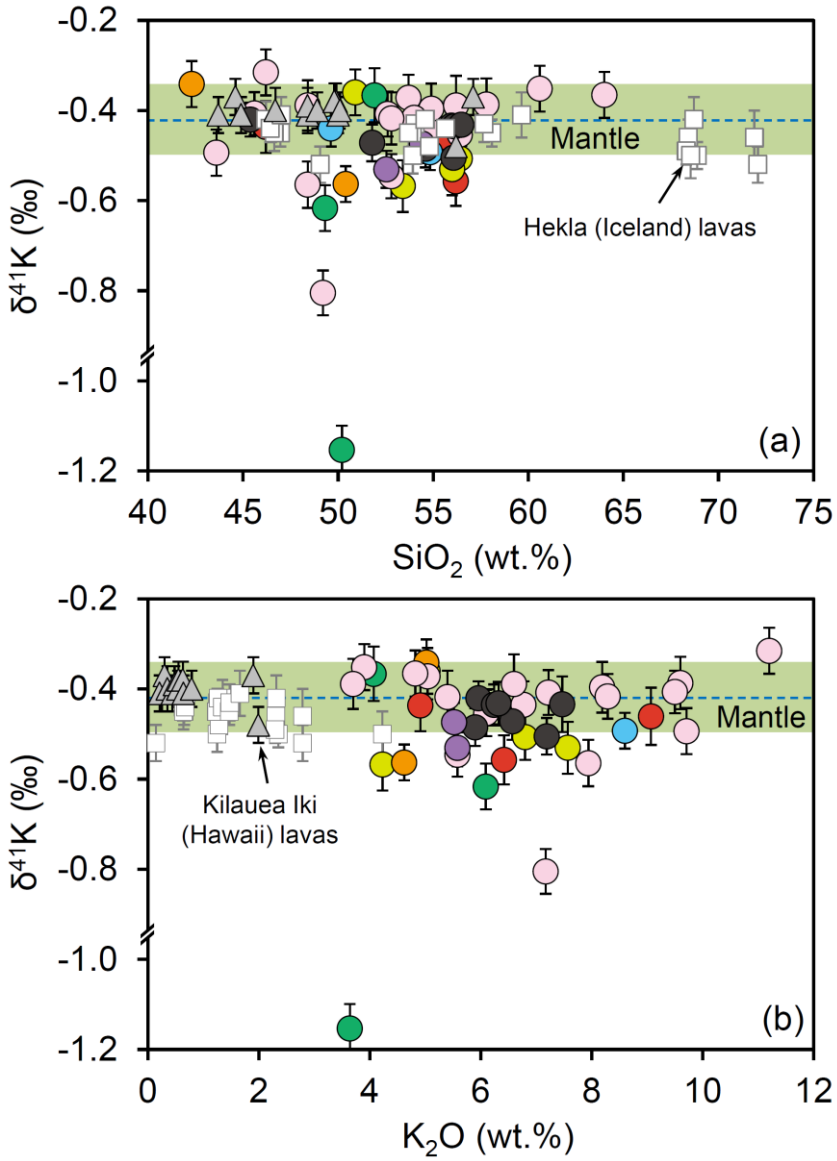

Figure S-3 Plots of $\delta^{41}K$ against **(a)** SiO_2 and **(b)** K_2O. Data for basaltic-rhyolitic lavas from Hekla volcano (Iceland) and Kilauea Iki lava lake (Hawaii) are also shown for comparison (Tuller-Ross *et al.*, 2019; Hu *et al.*, 2021). Horizontal dashed line and bar represent the $\delta^{41}K$ of the mantle (–0.42 ± 0.08 ‰; Hu *et al.*, 2021). The absence of correlation between $\delta^{41}K$ and SiO_2 or K_2O in K-rich volcanic rocks from the AHOB suggests insignificant K isotope fractionation during fractional crystallisation of these magmas.

Supplementary Information References

Barnekow, P. (2000) Volcanic rocks from central Italy: An oxygen isotopic microanalytical and geochemical study. Ph.D. thesis, University of Göttingen, 90 pp.

Chen, H., Tian, Z., Tuller-Ross, B., Korotev, R.L., Wang, K. (2019) High-precision potassium isotopic analysis by MC-ICP-MS: an inter-laboratory comparison and refined K atomic weight. *Journal of Analytical Atomic Spectrometry* 34, 160–171.

Guo, Z., Hertogen, J., Liu, J., Pasteels, P., Boven, A., Punzalan, L., He, H., Luo, X., Zhang, W. (2005) Potassic Magmatism in Western Sichuan and Yunnan Provinces, SE Tibet, China: Petrological and Geochemical Constraints on Petrogenesis. *Journal of Petrology* 46, 33–78.

Hu, Y., Chen, X.-Y., Xu, Y.-K., Teng, F.-Z. (2018) High-precision analysis of potassium isotopes by HR-MC-ICPMS. *Chemical Geology* 493, 100–108.

Hu, Y., Teng, F.-Z., Plank, T., Chauvel, C. (2020) Potassium isotopic heterogeneity in subducting oceanic plates. *Science Advances* 6, eabb2472.

Hu, Y., Teng, F.-Z., Chauvel, C. (2021) Potassium isotopic evidence for sedimentary input to the mantle source of Lesser Antilles lavas. *Geochimica et Cosmochimica Acta* 295, 98–111.

Li, X., Han, G., Zhang, Q., Miao, Z. (2020) Optimal separation method for high-precision K isotope analysis by using MC-ICP-MS with a dummy bucket. *Journal of Analytical Atomic Spectrometry* 35, 1330–1339.

Liu, D., Zhao, Z., Zhu, D.-C., Niu, Y., Widom, E., Teng, F.-Z., DePaolo, D.J., Ke, S., Xu, J.-F., Wang, Q. (2015) Identifying mantle carbonatite metasomatism through Os–Sr–Mg isotopes in Tibetan ultrapotassic rocks. *Earth and Planetary Science Letters* 430, 458–469.

Liu, S.A., Wang, Z.Z., Yang, C., Li, S.G., Ke, S. (2020) Mg and Zn isotope evidence for two types of mantle metasomatism and deep recycling of magnesium carbonates. *Journal of Geophysical Research: Solid Earth*, e2020JB020684.

McDonough, W.F., Sun, S.-S. (1995) The composition of the Earth. *Chemical Geology* 120, 223–253.

Morgan, L.E., Ramos, D.P.S., Davidheiser-Kroll, B., Faithfull, J., Lloyd, N.S., Ellam, R.M., Higgins, J.A. (2018) High-precision $^{41}K/^{39}K$ measurements by MC-ICP-MS indicate terrestrial variability of $\delta^{41}K$. *Journal of Analytical Atomic Spectrometry* 33, 175–186.

Plank, T. (2014) 4.17 – The chemical composition of subducting sediments. In: Holland, H.D., Turekian, K.K. (Eds.) *Treatise on Geochemistry*. Second Edition, Elsevier, Oxford, 607–629.

Prelević, D., Foley, S.F., Romer, R.L., Cvetković, V., Downes, H. (2005) Tertiary ultrapotassic volcanism in Serbia: constraints on petrogenesis and mantle source characteristics. *Journal of Petrology* 46, 1443–1487.

Prelević, D., Foley, S.F., Romer, R., Conticelli, S. (2008) Mediterranean Tertiary lamproites derived from multiple source components in postcollisional geodynamics. *Geochimica et Cosmochimica Acta* 72, 2125–2156.

Prelević, D., Akal, C., Foley, S.F., Romer, R.L., Stracke, A., Van Den Bogaard, P. (2012) Ultrapotassic mafic rocks as geochemical proxies for post-collisional dynamics of orogenic lithospheric mantle: the case of southwestern Anatolia, Turkey. *Journal of Petrology* 53, 1019–1055.

Prelević, D., Akal, C., Romer, R.L., Mertz-Kraus, R., Helvacı, C. (2015) Magmatic response to slab tearing: constraints from the Afyon Alkaline Volcanic Complex, Western Turkey. *Journal of Petrology* 56, 527–562.

Rudnick, R., Gao, S. (2014) 4.1 – Composition of the continental crust. In: Holland, H.D., Turekian, K.K. (Eds.) *Treatise on Geochemistry*. Second Edition, Elsevier, Oxford, 1–51.

Tuller-Ross, B., Savage, P.S., Chen, H., Wang, K. (2019) Potassium isotope fractionation during magmatic differentiation of basalt to rhyolite. *Chemical Geology* 525, 37–45.

Xu, Y.-K., Hu, Y., Chen, X.-Y., Huang, T.-Y., Sletten, R.S., Zhu, D., Teng, F.-Z. (2019) Potassium isotopic compositions of international geological reference materials. *Chemical Geology* 513, 101–107.

Zhao, Z., Mo, X., Dilek, Y., Niu, Y., DePaolo, D.J., Robinson, P., Zhu, D., Sun, C., Dong, G., Zhou, S. (2009) Geochemical and Sr–Nd–Pb–O isotopic compositions of the post-collisional ultrapotassic magmatism in SW Tibet: petrogenesis and implications for India intra-continental subduction beneath southern Tibet. *Lithos* 113, 190–212.